Poly(ethylene glycol)-Based Thiol-ene Hydrogel Coatings—Curing Chemistry, Aqueous Stability, and Potential Marine Antifouling Applications

Pontus Lundberg,[†] Anouk Bruin,[‡] Job. W. Klijnstra,[‡] Andreas M. Nyström,[§] Mats Johansson,[†] Michael Malkoch,[†] and Anders Hult*[,†]

KTH Fibre and Polymer Technology, Teknikringen 56-58, SE-100 44 Stockholm, Sweden, TNO Science and Industry, Bevesierweg (Harssens), P.O. Box 505, 1780 AM Den Helder, The Netherlands, and Swedish Medical Nanoscience Center, Department of Neuroscience, Karolinska Insitutet, Retzius väg 8, S-171 77 Stockholm, Sweden

ABSTRACT Photocured thiol-ene hydrogel coatings based on poly(ethylene glycol) (PEG) were investigated for marine antifouling purposes. By varying the PEG length, vinylic end-group, and thiol cross-linker, a library of hydrogel coatings with different structural composition was efficiently accomplished, with or without ester linkages. The thiol-methacrylate and thiol-allyl systems were evaluated with respect to curing, degradation, as well as antifouling properties. Methacrylate-based systems exhibited homopolymerization, whereas allyl-based systems reacted more selectively through thiol-ene couplings reaction. The ester-free hydrogels elucidated higher hydrolytic stability whereas longer PEG chains accelerated the degradation process. The antifouling properties were evaluated by protein adsorption with Bovine serum albumin (BSA) and bioassays with the marine bacteria, *Cobetia marina*, and the marine diatom, *Amphora coffeaeformis*; in all tests, longer PEG lengths improved the antifouling properties.

KEYWORDS: thiol-ene chemistry • photocuring • hydrogels • degradation • antifouling • bioassays

INTRODUCTION

Submerging a surface into a marine or freshwater environment will lead within minutes to the adhesion of biological macromolecules such as proteins, polysaccharides, and proteoglycans. The adhered layer acts as a conditioner for marine bacteria and diatoms, which will adhere in a second stage of fouling and occur within 24 h after submersion. The adhered microbes will subsequently form a microbial biofilm that allows the settlement of spores of microalgae to further facilitates the settlement of macroorganisms such as barnacles (1, 2). The adherence and subsequent colonization of a surface creates a number of problems, e.g., accelerated rate of degradation or corrosion as well as increased drag resistance due to surface roughening. The increase in surface roughness is mainly caused by the macrofoulers and can entail enormous costs in both time and money. An illustrative example of the numbers involved was formulated by Hare (3) in 1998, who estimated that a supertanker will lose about 2 days of service each year, corresponding to a loss of approximately $125000 per year, if the ship has insufficient protection against fouling. The loss in speed can be circumvented by increasing the power of the propellers. This increase in power will, however, lead to an increase in fuel consumption thus giving higher costs, and Hare stated that a cruiser will require about 45% more fuel after 6 months in temperate waters (3).

Early surface protection approaches included natural products such as wax, tar, and asphalt, and later on copper and other heavy metals were used, with limited success. The most efficient antifouling coatings to date are the self-polishing-tributyltin (SP-TBT) systems, which were used with great success until the final ban on January first 2008 (4). By then, it was clear that TBT caused severe damage on nontarget organisms and accumulated into toxic levels in busy harbors (1−3, 5). Because of the upcoming ban, the last decades of research have been focused on finding alternatives to TBT; however, none of the alternatives has so far proven as efficient as TBT. One of the most commonly used antifouling agents has been CuO but a debate on the environmental impact of copper has arisen, which has led to restrictions in the use of copper in the Baltic Sea, for instance.

As a result of intensified research, a number of novel strategies for designing antifouling marine coatings have arisen, of which fouling release coatings are among the most promising biocide-free alternatives. For an extensive review of the current research, the reader is encouraged to read the recently published book edited by Hellio and Yebra (5). These biocide-free coatings are based on creating a surface

* To whom the correspondence should be addressed. Tel.: +46 8 790 8268. Fax: +46 8 790 8283. E-mail: andult@kth.se.
Received for review December 10, 2009 and accepted February 11, 2010
[†] KTH Fibre and Polymer Technology.
[‡] TNO Science and Industry.
[§] Karolinska Insitutet.
DOI: 10.1021/am900875g

to which fouling organisms have very poor adhesion. This can be achieved with hydrophobic materials such as silicones, which exhibit very low surface energy (2, 5, 6), or the complete opposite, surfaces that are very hydrophilic and become "stealthy" because of the fact that there is no difference in energy between the surrounding water and the surface and thereby minimize the thermodynamic driving force for irreversible binding. In the literature, such hydrophilic surfaces have been designed as cross-linked hydrogels that swell in contact with water. For example, Cowling et al. (7) and Cowie et al. (8) utlized poly(2-hydroxyethyl methacrylate) (PHEMA)-based hydrogels. These systems have been field tested, but without the addition of biocides, the coatings had poor antifouling properties. Rasmussen et al. (9, 10) evaluated alginate, chitosan, polyvinyl alcohol and agarose hydrogels in laboratory tests with barnacles and marine bacteria, and concluded that all tested hydrogels had lower settlement than polystyrene surfaces, and that the differences between the gels were due to inherent chemical differences in the polymer network rather than variation of modulus and hydrophilicity. Gudipati et al. (11) reported on the preparation of copolymer gels consisting of hyperbranced fluoropolymers and poly(ethylene glycol) (PEG) with the ability to resist adsorption of a range of biomacromolecules and inhibiting settlement of zoospores of the marine algae *Ulva*. In a recent study, Ekblad et al. (12) studied the antifouling properties of a copolymer gel consisting of HEMA and poly(ethylene glycol) methacrylate (PEGMA) which showed promising performance with respect to a wide range of fouling species. The antifouling properties of the copolymer gel were attributed to the stealth characteristics of the PEG component, consistent with a wide range of studies of PEGylation of surfaces and nanoparticles in the field of biomedicine (13).

PEGylated surfaces are known for their resistance to protein adsorption, which is attributed to their strong interaction with water, charge neutrality and absence of hydrogen donors (14, 15). However, the mechanisms resulting in protein-resistant PEG-based surfaces are not fully known. For example, there is a debate regarding the required molecular weight of the PEG on the surface. Should the surface consist of high molecular weight PEG with high chain mobility or a dense surface of short PEG oligomers (14, 15)? The most common method for cross-linking PEG chains into a hydrogel is to use acrylated PEGs which are cross-linked by free radical mechanisms (11, 16−18). Such a reaction results in a poorly controlled hydrogel structure and as a consequence the construction of an inhomogeneous network. To achieve better structural control, Malkoch et al. (19) reported on the utilization of the highly efficient click reaction (20) for the construction of more homogeneous PEG hydrogels. The concept took advantage of the CuAAC catalyzed click reaction between azides and alkynes (21, 22) to cross-link networks of telechelic PEG-chains. This type of reaction is, however, poorly suited for the design of a biocide-free coating for antifouling applications because copper, which is used as a catalyst, is a known biocide. Instead, the thiol-ene coupling reaction, fulfilling the criteria of click chemistry, is more suitable and the approach. The chemistry can take place with or without the use of an initiator and by heating, radiating with UV light or even spontaneously (23, 24). After being almost forgotten for a few decades, due to bad odor and yellowing of films, the thiol-ene reaction has recently become a popular reaction due to the development of novel initiators that has eliminated the problem with yellowing. The step-growth mechanism of the thiol-ene reaction enables a homogeneous network buildup which in combination with the insensitivity to oxygen inhibition, suggests that thiol-ene systems are ideal for coating applications. Reports dealing with conetworks of PEG based on thiol-ene chemistry have been published (25, 26) and recently Rydholm et al. (27−29) reported the synthesis and degradation of PEG-based hydrogel materials synthesized by thiol−ene chemistry for biomedical applications. Another recent example of cross-linked PEG based materials were published by Li et al. (30) who investigated the difference in reactivity and film properties between PEG vinyl ethers and PEG vinyl esters cross-linked with different thiols.

In this work, we have focused our attention on preparing "stealthy" hydrophilic surfaces based on hydrogels of PEG prepared via thiol-ene cross-linking chemistry intended for marine antifouling applications. By varying the PEG chain length, cross-linker as well as cross-linking chemistry, a library of coatings has been formulated and evaluated with respect to their curing behavior, thermal properties, swelling/degradation behavior as well as their ability to resist protein adsorption and settlement of marine bacteria and diatoms.

EXPERIMENTAL SECTION

Materials. Tetraethylene glycol dimethacrylate (technical, >90%) (**1T**) and poly(ethylene glycol) dimethacrylate (Mn ∼ 750) (**1P**) was obtained from Sigma-Aldrich. CH_2Cl_2 (p.a), tetrahydrofuran (THF) (p.a.), methanol (p.a.), heptanes (p.a.)), and ethyl acetate (EtOAc) (EMPROVE exp) were obtained from Merck and ethanol (EtOH) (96%) was obtained from VWR. $MgSO_4$ and silica gel for flash chromatography were obtained from Acros Organics. Allyl bromide 99% (Alfa Aesar), tris(2-(3-mercaptopropionyloxy)ethyl) isocyanurate (**4**) (Wako), Thiocure ETTMP 700 (**6**) (Bruno Bock). All other chemicals were used as received from Sigma-Aldrich. 4-(Dimethylamino) pyridinium 4-toluenesulfonate (DPTS) was prepared as reported elsewhere (31). Artificial seawater (ASW) was prepared from Instant Ocean (Aquarium Systems).

Methods. ***Nuclear Magnetic Resonance (NMR).*** ^1H and ^{13}C NMR was performed on a Bruker Avance 400 MHz instrument using $CDCl_3$ as a solvent and TMS as internal reference.

Infrared Spectroscopy (IR). IR spectra were recorded on a Perkin-Elmer Spectrum 2000 FTIR equipped with a heat-controlled single reflection attenuated total reflection (ATR) accessory from Specac Ltd.

Raman Spectroscopy. Raman spectra were acquired for all samples using a Perkin-Elmer Spectrum 2000 NIR FT-Raman instrument. Each spectrum was based on 32 scans using 1500 mW laser power. The conversion of thiols (2573−2568 cm^{-1}) or alkene (1646 cm^{-1} methacrylate, 1640 cm^{-1} allyl ether) was determined using either the triazine ring (1610 cm^{-1}) or the ester bond (1730 cm^{-1}) as internal reference.

Contact Angle Goniometry. Static contact angle measurements were performed on a KSV Instruments CAM 200 equipped with a Basler A602f camera, using 5 μL droplets of MiliQ water

and a relative humidity of 50%. Determination of the contact angles was performed using CAM software. To determine the contact angle of a coating, three coated glass slides were used and on each slide the following procedure was used. A drop was automatically dispensed and placed on the coating and the first picture was taken 5 s after placing the drop. Additionally, two pictures were taken after 7 and 9 s, respectively. On each coating, three drops were placed 5 mm apart and photographed.

Fluorescence Spectroscopy. Fluorescence spectroscopy for protein adsorption measurements was performed using a Zeiss Axiplan 2 imaging equipped with a CCD-camera and AxioVision 4.7 software.

Synthesis of 4-(2-(Allyloxy)ethoxy)-4-oxobutanoic Acid (AEOBA). 100 g (979 mmol) of 2-allyloxyethanol and 23.9 g (198 mmol) of DMAP were dissolved in a mixture of 100 mL of CH_2Cl_2 and 10 mL of pyridine. The solution was cooled with an ice bath to 0 °C and 117.6 g (1175 mmol) of succinic anhydride was added in portions. The reaction was subsequently removed from the ice batch and stirred overnight. A small aliquot of the crude mixture was taken out and analyzed by ^{1}H NMR and ^{13}C NMR to validate the complete disappearance of the methylene next to the hydroxyl group and that the carbonyls remaining corresponding to an excess of succinic anhydride could be seen. Twenty milliliters of H_2O was added in order to quench the anhydride and the disappearance of the carbonyls from succinic anhydride was monitored using ^{13}C NMR. The crude mixture was purified by extraction with 3 × 50 mL 10% $NaHSO_4$, whereafter the organic phase was dried with $MgSO_4$ and the solvent was evaporated. The product (**AEOBA**) was obtained as a slightly yellow oil with a yield of 95% (189 g). ^{1}H NMR δ (ppm) = 2.68 (m, −(O=)C−C**H**$_2$−C**H**$_2$−C(=O)−, 4H), 3.65 (t, 2H, J = 8 Hz, −O−C**H**$_2$−CH$_2$−O−C(=O)−), 4.03 (d, 2H, J = 8 Hz, =CH−C**H**$_2$−O−), 4.27 (t, 2H, J = 8 Hz, −O−CH$_2$−C**H**$_2$−O−C(=O)−), 5.25 (m, 2H, **H**$_2$C=C−), 5.90 (m, 1H, =C**H**−). ^{13}C NMR δ (ppm) = 29.13, 64.19, 67.98, 72.35, 117.73, 134.53, 172.49, 177.42.

General Procedure for Allyl Ether Functionalization of PEGs Based on DCC Ester Chemistry (2). Two different lengths of PEG were functionalized with allyl ethers using DCC chemistry. The product based on PEG with DP = 4 is called **2T** and the product based on PEG with DP ≈ 14 (MW 570−630 g mol^{-1}) **2P**. To synthesize **2T**, we charged a 100 mL round-bottom flask with 10.0 g (51.5 mmol) of PEG (DP = 4) dissolved in 25 mL of CH_2Cl_2, 1.26 g (10.3 mmol) of DMAP, and 3.0 g (10.3 mmol) of DPTS and added 25.0 g (124 mmol) of **AEOBA**. The solution was cooled to 0 °C in an ice bath, followed by slow addition of 23.4 g (113 mmol) of DCC. The reaction was allowed to proceed overnight before the solid residues were filtered off and discarded and the solvent was evaporated. The crude product was subsequently purified using flash chromatography eluting with gradient mixtures of heptane:EtOAc from 1:0 to 2:8 to give the pure product (**2T**) as a slightly yellow oil. Yield 22.6 g (78%) **2T** ^{1}H NMR δ (ppm) = 2.68 (m, 8H, −(O=)C−C**H**$_2$-C**H**$_2$-C(=O)−), 3.66 (m, 16H, −O-C**H**$_2$−C**H**$_2$−O−) 3.70 (t, 4H, J = 8 Hz, −O−C**H**$_2$−CH$_2$−O−C(=O)−), 4.03 (d, 4H, J = 4 Hz, =CH−C**H**$_2$−O−), 4.27 (m, 4H, −O−CH$_2$−C**H**$_2$−O−C(=O)−), 5.25 (m, 4H, **H**$_2$C=C−), 5.90 (m, 2H, =C**H**−. ^{13}C NMR δ (ppm) = 29.14, 64.00, 64.06, 67.94, 70.73, 117.59, 134.53, 172.40. FT-IR (cm^{-1}): 2869, 1731 ($\nu_{C=O}$), 1646 ($\nu_{C=C}$), 1452, 1409, 1384, 1248, 1209, 1159, 1106, 1037, 994, 926, 858, 639. Raman (cm^{-1}): 3085, 3013, 2937, 2875, 1736 ($\nu_{C=O}$), 1645 ($\nu_{C=C}$), 1453, 1422, 1288, 1243, 1130, 1073, 992, 860.

2P was synthesized according to the general procedure outlined for (**2**). Yield: 20.4 g (61%). **2P** ^{1}H NMR δ (ppm) = 2.68 (m, 4H, −(O=)C−C**H**$_2$−C**H**$_2$−C(=O)−), 3.66 (m, 56H, −O-C**H**$_2$−C**H**$_2$−O−) 3.70 (t, 4H, J = 12 Hz, −O−C**H**$_2$−CH$_2$−O−C(=O)−), 4.03 (d, 4H, J = 4 Hz, =CH−C**H**$_2$−O−), 4.27 (m, 4H, −O−CH$_2$−C**H**$_2$−O−C(=O)−), 5.25 (m, 4H, **H**$_2$C=C−), 5.90 (m, 2H, =C−). ^{13}C NMR δ (ppm) = 29.15, 64.02, 64.04, 67.95, 10.71, 117.62, 134.53, 172.42. FT-IR (cm^{-1}): 2866, 1731 ($\nu_{C=O}$), 1646 ($\nu_{C=C}$), 1452, 1409, 1384, 1248, 1209, 1097, 1036, 994, 932, 858. Raman (cm^{-1}): 3084, 3010, 2937, 2875, 1738 ($\nu_{C=O}$), 1646 ($\nu_{C=C}$), 1471, 1422, 1288, 1244, 1130, 1039, 992, 860.

General Procedure for Allyl Ether Functionalization of PEGs Based on Alkoxide-Allylbromide Ether Chemistry (3). Two different lengths of PEG were functionalized with allyl ethers using alkoxide-allylbromide of PEG. The product based on PEG with DP = 4 is called **3T** and the product based on PEG with DP ≈ 14 **3P**. To synthesize **3T**, a 100 mL round-bottom flask was charged with 20.0 g (103 mmol) of PEG and the PEG was dissolved in 30 mL THF and cooled to 0 °C before 5.93 g (247 mmol) of NaH was added to form Na-alkoxylates. After stirring for 30 min, 32.4 g (268 mmol) of allyl bromide was added. The reaction mixture was then allowed to reach room temperature and stirred overnight. The product was subsequently purified using flash chromatography with gradient mixtures of heptane:EtOAc from 1:0 to 2:8 to give the pure product (**3T**) as slightly yellow oil. Yield: 23.1 g (82%). **3T** ^{1}H NMR δ (ppm) = 3.60 (m, 4, =C−CH−O−C**H**$_2$−), 3.66 (m, 16H, −O−C**H**$_2$−C**H**$_2$−O−), 4.03 (d, 4H, J = 4 Hz, =CH−C**H**$_2$−O−), 5.25 (m, 4H, **H**$_2$C=C−), 5.90 (m, 2H, =C**H**−). ^{13}C NMR δ (ppm) = 69.61, 70.78, 70.81, 72.40, 117.23, 134.95. FT-IR (cm^{-1}): 2863, 1646 ($\nu_{C=C}$), 1451, 1421, 1347, 1292, 1249, 1095, 1037, 994, 921, 879, 846. Raman (cm^{-1}): 3083, 3015, 2981, 2938, 2910, 1646 ($\nu_{C=C}$), 1470, 1422, 1288, 1241, 1129, 915, 882, 844.

3P was synthesized according to the general procedure outlined for (**3**). Yield: 15.6 g (69%). **3P** ^{1}H NMR δ (ppm) = 3.60 (m, 4, =C−CH−O−C**H**$_2$−), 3.66 (m, 56H, −O−C**H**$_2$−C**H**$_2$−O−), 4.03 (m, 4H, =CH−C**H**$_2$−O−), 5.25 (m, 4H, **H**$_2$C=C−), 5.90 (m, 2H, =C**H**−). ^{13}C NMR δ (ppm) = 69.61, 70.76, 70.81, 72.41, 117.26, 134.95. FT-IR (cm^{-1}): 2863, 1646 ($\nu_{C=C}$), 1451, 1421, 1347, 1292, 1249, 1095, 1037, 994, 921, 879, 846. Raman (cm^{-1}): 3083, 3015, 2981, 2938, 2910, 1646 ($\nu_{C=C}$), 1470, 1422, 1288, 1241, 1129, 915, 882, 844.

Synthesis of 1,3,5-Tris(3-mercaptopropyl)-1,3,5-triazinane-2,4,6-trione (5). 15.0 g (60.2 mmol) of 1,3,5-triacryloylhexahydro-1,3,5-triazine and 41.2 g (542 mmol) of thioacetic acid and 0.99 g (6.02 mmol) of 2,2′-azobis(2-methylpropionitrile) were charged in a 250 mL round-bottom flask equipped with a cooler. The reaction was allowed to proceed at 60 °C for 6 h, after which 50 mL of methanol and 25 mL of concentrated HCl were added to the reaction mixture, which was left to proceed at 60 °C overnight. The reaction was cooled to ambient temperature, and 100 mL of H_2O and 400 mL of CH_2Cl_2 were added. The phases were separated and the organic phase was retained and subsequently washed with 3 × 100 mL H_2O. The organic phase was dried with $MgSO_4$ and the solvent evaporated followed by further purification by flash chromatography with gradient heptanes: EtOAc mixtures from 1:0 to 2:8 and the product was received as a slightly yellow, highly viscous oil. Yield: 14.2 g (67%). ^{1}H NMR δ (ppm) = 1.55 (t, 3H, J = 16 Hz, −S**H**), 1.98 (quintet, 6H, J = 28 Hz, −CH$_2$−C**H**$_2$−CH$_2$−), 2.57 (q, 6H, J = 24 Hz, −C**H**$_2$−SH) 4.02 (t, 6H, J = 16 Hz, >N−C**H**$_2$−CH$_2$−). ^{13}C NMR δ (ppm) = 22.13, 32.04, 42.01, 149.20. FT-IR (cm^{-1}): 2964, 2567 (ν_{S-H}), 1682 ($\nu_{C=O}$ triazine ring), 1455, 1422, 1374, 1334, 1319, 1288, 1251, 1134, 1066, 857, 761, 659. Raman (cm^{-1}): 3006, 2965, 2890, 2820, 2568 (ν_{S-H}), 1755 ($\nu_{C=O}$ triazine ring), 1430, 1373, 1321, 1290, 1252, 1201, 1136, 1044, 866, 748, 694, 661.

Preparation of Glass Surfaces. Microscope slides with cut edges (76 × 26 mm, Thermo Scientific, Menzel-Gläser) were cleaned by immersion in household detergent, Yes (Procter & Gamble). To further clean the slides they were immersed in a solution of HCl:H_2O_2:H_2O (1:1:5). The slides were rinsed with deionized water and EtOH followed by immersion in EtOH, where they were stored until further use. To avoid detachment of the coatings, the slides were functionalized with thiol groups. The slides were submerged for 10 min in a 1:1 H_2O:EtOH

solution containing 0.05% glacial acetic acid and 0.4% 3-mercaptopropyl trimethoxysilane followed by air drying in a LAF bench. To cure the silane, the slides were placed in an oven at 115 °C for 10 min followed by immersion in EtOH. Before coating, the slides were wiped using Durx 670 cleanroom wipers soaked in EtOH followed by thorough rinsing with EtOH and air drying in a LAF bench.

General Coating Procedure. Equimolar amounts of methacrylates/allyls and thiols with a total dry content of 3.2 g were weighed and diluted with 400 mg of butyl acetate; 0.5 wt% of Irgacure 184 was added and the solution was mixed to a homogeneous solution using a vortexer. The dry slides were subsequently coated using an Ericsen applicator with a gap of 60 μm, with each 3.2 g batch yielding 10−15 coated slides. The coated slides were left to flash off the solvent for 1 h before UV-induced polymerizations were performed using a Fusion UV Curing System model F300 equipped with Fusion electrodeless bulbs standard type BF9 (Lamp power 300 W/inch, 1800 W total). The films were cured by 15 successive passes under the lamp to give a total dose of 500 mJ/cm^2 as determined by measuring the intensity with a UVICURE Plus from EIT Inc., Sterling, VA.

Swelling and Stability Studies. Gravimetric and contact-angle measurements were performed to evaluate the swelling and stability of the coatings. The gravimetric studies were performed by weighing the glass slides before and after coating formation to determine the dry weight of the film. Three slides of each coating system were subsequently submerged in deionized water (DIW) and ASW, respectively. After 1 day of submersion, the slides were taken up and gently dried and weighed, after which contact angle measurements were performed. This procedure was repeated on day 2, 3, 4, 9, 15, and 28. (On day 15, only gravimetric analysis was performed, as the contact angle equipment was out of order).

Protein Adsorption Studies. Protein adsorption studies were performed after swelling the coatings in 25 mL of phosphate buffer solution (PBS) for 1 h. The coatings were subsequently incubated by placing 500 μL drops of 0.1 mg/mL FITC labeled BSA in PBS on the top of the coatings. After 10 min of incubation, the coatings were rinsed with 20 mL of PBS and immediately imaged using a fluorescence microscope. Duplicate images of each coating before and after incubation with BSA were recorded. The total fluorescence was determined using the built-in FITC filter of the microscope, with a constant exposure time, magnification, and image area for all the surfaces. To calculate the total fluorescence from BSA, the background fluorescence for each coating type was first subtracted using ImageJ software and the total fluorescence was calculated using the built-in plug-in.

Bioassays. ***Bacterial Assay.*** The bacterial suspension of the marine bacteria *Cobetia marina*, used for the testing was obtained after the cells were repeatedly washed with PBS and centrifuged to remove excess EPS for optimal adhesion.

The conditioned replicate slides were immersed for 1 h in polystyrene quadriPERM plates (GreinerBio-one Ltd.) containing 8 mL suspension of *C. marina* bacteria with an OD of 0.2 (595 nm). The slides were incubated on a shaker (150 rpm) for 1 h at 28 °C. Nonadhered and loosely attached cells were removed by dipping the slides once in sterile seawater. The slides were transferred back into quadriPERM plates containing 8 mL of sterile SW with added growth medium and incubated again for 4 h at 28 °C under gentle shaking (150 rpm). At the end of incubation, the slides were rinsed again and then placed into slide holders and partially air-dried. Attached cells were stained, using the fluorochrome SYTO13 (1.5 mM), for biomass quantification in a Tecan plate reader (GENios, Magellan software) Biomass quantification on acid-washed glass (hydrophilic) and Silastic T2 (hydrophic) was also determined and used as reference substrates to which settlement responses on the coatings could be compared.

To quantify the adhesion strength of attached bacteria, we used a rotating drum test. Slides were treated as above. After the growth step replicate slides of each coating were rotated on the rotating drum for 10 min at 12 knots in natural seawater. This rotational speed of the drum exposes the bacteria to shear stress (turbulent flow), causing an amount of bacteria to be removed from the surfaces. The remaining bacteria were then quantified using SYTO13 stain as described above. Data are expressed as % biofilm removal (Δ biomass/biomass before release × 100%).

One sample of the TNO references and one sample of each coating were exposed without bacteria under the same conditions as the other samples to serve as coating blanks to check for autofluorescence and contamination.

Diatom Assay. The common fouling species *Amphora coffeaeformis* was used for this test. Diatom cultures were maintained in the growth room at TNO (18 °C and 24 h light exposure) in enriched filtered sterilized seawater with silicate-enriched F2 growth medium. Eighty microliters of diatom cell suspension grown for 3−4 days was placed in a line over the samples.

The samples were incubated for 2 h in the dark to allow the cells to attach to the surface. The diatom slides were then gently dip-rinsed with sterile seawater to remove unattached diatoms. Diatom fluorescence on the slides was measured using the Tecan plate reader (GENios, Magellan software). The slides were transferred into quadriPERM plates containing 10 mL sterile, filtered seawater with added growth medium and incubated for 5 days at 18 °C with 24 h light exposure. After the incubation period, the slides were removed, gently dip-rinsed in sterile seawater and the fluorescence was then remeasured using the Tecan plate reader. Replicated samples were evaluated and compared with acid-washed glass controls and the hydrophobic TNO standard Silastic T2.

RESULTS AND DISCUSSION

Synthesis of Monomers and Cross-Linker. To fully understand the impact of curing chemistry on the thermal and antifouling properties of the coatings, allyl functional PEGs were synthesized, formulated, and compared to the commercially available TEGDMA and PEGDMA. Consequently, allylic PEGs comprising ester groups, **2**, and exclusively ether bonds, **3**, were synthesized to determine their effect on structural stability of developed coatings. The synthesis of allylated PEGs with ester linkages (**2T**, DP = 4; **2P**, DP ≈ 14) was achieved by an esterification reaction with **AEOBA** using DCC dehydration chemistry. After filtering off the DC-urea byproducts and purification using column chromatography, the pure products were obtained according to ^{1}H NMR and ^{13}C NMR. FT-IR and FT-Raman analysis further confirmed the structures, displaying peaks from the carbonyl (C═O stretch) at 1717 cm^{-1} and the allyl (C═C stretch) at 1638 cm^{-1} (see Figures S1 and S2 in the Supporting Information). Synthesis of ester free allylated PEGs (**3T**, DP = 4; **3P**, DP ≈ 14) was accomplished by adding NaH to a solution of PEG in THF producing the alkoxylate followed by the addition of allyl bromide. After purification using column chromatography, the obtained products were pure according to ^{1}H NMR and ^{13}C NMR. IR and Raman spectroscopy further confirmed the presence of allyl groups (C═C stretch at 1645 cm^{-1}) (see Figures S1 and S2 in the Supporting Information).

Table 1. Properties of Starting Materials, Hydrogel Coatings, and Reference Materials

entry	PEG	thiol	conv. SH (%)	conv. C=C (%)	T_g (°C)	T_c(°C)	ΔH_c(J g^{-1})	T_m(°C)	ΔH_m (J g^{-1})	contact angle (deg)	Biofilm release as % removal
1T											
1P						−12.3	83.4	9.3	85.6		
2T					−63.9						
2P					−60.7	−42.0[a]	61.9	6.3	69.9		
3T						−38.7	119.8	−26.8	125.5		
3P						0.2	124.9	22.0	130.7		
4					−41.5						
5					−50.9						
6					−65.0						
H1	1T	4	45	>95	−2.9					64 ± 2	50
H2	1P	4	56	>95	−33.9					48 ± 2	59
H3	1P	6	61	86	−44.0					45 ± 2	29
H4	1T	6	73	>95	−36.4					35 ± 4	41
H5	2T	4	>95	>95	−24.1					68 ± 2	68
H6	2P	4	>95	>95	−36.3					50 ± 1	19
H7	3T	5	88	>95	−39.4					50 ± 6	
H8	3P	5	>95	92	−54.1	−25.2[a]	21.7	5.7	20.8	57 ± 2	
glass										14 ± 1	76
primed glass										49 ± 4	
silastic T2											71

[a] Crystallization occurred during the heating cycle.

To exclusively produce an ether-based hydrogel, we synthesized an ester-free 1,3,5-tris(3-mercaptopropyl)-1,3,5-triazinane-2,4,6-trione cross-linker **5**. This was achieved by a one-pot, two-step, procedure. In the first step, 1,3,5-triacryloylhexahydro-1,3,5-triazine and thioacetic acid were reacted through a thiol-ene reaction followed by hydrolytical cleavage of the thioester in the second step. An oily compound **5** was obtained in 67% yield after column chromatography purification. Analysis by ^{1}H NMR and ^{13}C NMR confirmed the purity of the product. In IR and Raman analyses, the presence of peaks from the carbonyl in the triazine ring (C=O stretch) at 1755 cm^{-1} and the thiol (S−H stretch) at 2568 cm^{-1} further confirmed that **5** had been formed.

Hydrogel Coating Preparation, Curing, and Physical Properties. Eight hydrogel coatings, **H1**−**H8**, were formulated, all have equimolar amounts of thiols to unsaturated PEGs (Table 1 and Figure 1) and to have a dry content of 90% in BuOAc. The formulations were chosen to allow a comparative study of the effect of different structural features in the formulations. **H1**, **H4**, **H5**, and **H7** all contain short PEG segments (DP = 4) in comparison to **H2**, **H3**, **H6**, and **H8** (DP ≈ 14). **H1**−**H4** are methacrylate based and **H5**-**H8** are allyl-based. In the case of **H5** and **H6**,the formulations include esters linkages, whereas **H7** and **H8** are purely ether-based. **H1**, **H2**, **H5**, and **H6** include a small ester-based thiol cross-linker **4**, whereas **H7** and **H8** employ an analogue without any ester linkages **5**. **H3** and **H4**, on the other hand, employ a more extended trifunctional thiol PEG with ester linkages.

Microscope slides were chosen as model substrates for the fabrication of hydrogels coating. To avoid detachment of the coatings, the slides were thiolated using 3-mercaptopropyl trimethoxysilane groups. The methacrylated PEGs systems **H1**−**H4** and the pure ether-based system **H7**−**H8** all elucidated good wetting properties, whereas allylated ester systems **H5**−**H6** required few seconds before evenly wetting the substrate. After flashing off the BuOAc for 1 h in ambient temperature, the coatings were cured under UV light at a total dose of 500 mJ/cm^2. Interestingly, systems **H1** and **H3**, comprising of the short PEG methacrylate, **1T**, and the ester based triazine trithiol, **4**, and of the long PEG methacrylate, **1P** and the TMP-PEG based trithiol, **6**, respectively, had slight top curing. Furthermore, the pure ether-based hydrogels **H7**−**H8** displayed shrinkage, especially **H7**. Systems **H2**, **H4**, **H5**, and **H6** were evenly cured with smooth and transparent films as a result while systems, making them almost invisible to the naked eye. All hydrogels were analyzed with both FT-Raman and FT-IR. FT-Raman is a very useful technique for monitoring alkene and thiol structures, thus giving information about conversion in the films. FT-IR, on the other hand, gives strong signals for carbonyls, hydroxyls, and carboxylic acids, making the technique suitable for monitoring the degradation of the coatings. Raman spectroscopy (Figure 2) revealed that all methacrylated systems retained residual thiol groups. In the case of **H1** and **H2**, thiol conversion reached only 45 and 56%, respectively. This was seen by the characteristic S−H stretch peak at 2573 cm^{-1}. In addition, the peak from the methacrylate double bond at 1683 cm^{-1} had completely disappeared, indicating that homopolymerization of the methacrylate groups had taken place. This is in good accordance with previous studies on thiol-methacrylate systems (23,32,33). Similar results were obtained for system **H3** (61% thiol conversion) and **H4** (73% thiol conversion), although system **H3** residual methacrylate groups (86% conversion) still

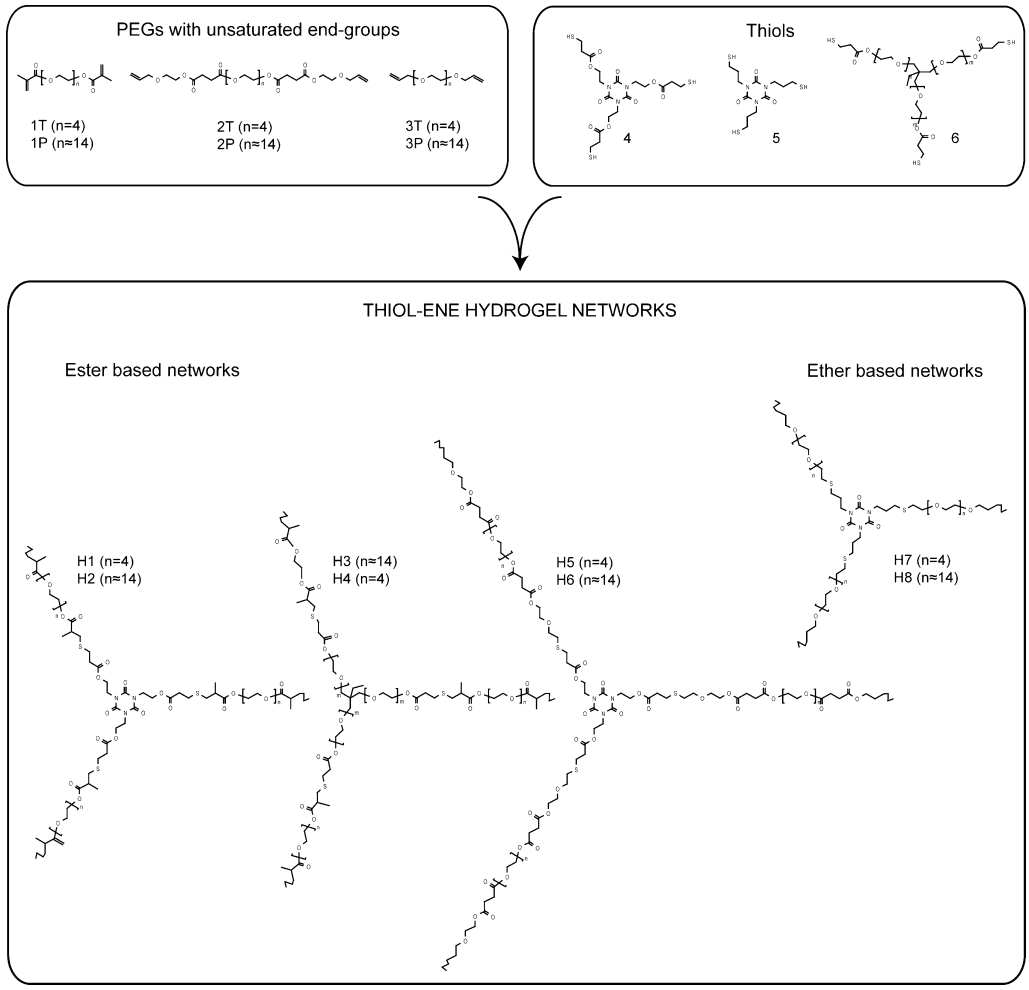

FIGURE 1. 1−3 PEGs with methacrylates or allyl functionalities and thiol cross-linkers 4−6 used for the formulation of hydrogel coatings. H1−H8 structures of different hydrogel coating formulations.

remained. In contrast, allylic systems **H5−H8** demonstrated complete conversion of both thiols and allyls (1645 cm^{-1}), indicating that a homogeneous thiol-allyl ether networks had formed. System **H7** contained small amounts of thiols, which may be due to some homopolymerization of the allyl ethers or inadequate equimolar ratio of thiols and enes during formulation preparation. The relatively high extent of homopolymerization in the thiol-methacrylate systems **H1−H4** is most likely a result of the tight structure formed rather than differences in reactivity between the methacrylate homopolymerization and the thiol methacryalte reaction, as the extent of homopolymerization is reduced with respect to increased length of PEG. This could further be supported by the results from **H7** where remaining thiols indicate homopolymerization of the allyl ethers. In the case of **H3**, where both thiols and methacrylates remained in the film after curing, the results can be due to the relatively low concentration of reactive groups as the PEG and cross-linker are extended and therefore decreasing the reaction efficiency.

Thermal Properties of Starting Materials and Hydrogels. To fully understand the intrinsic properties of the networks and the effect of building blocks on phase transitions, DSC analysis were performed on the starting materials and the cured films (Table 1). PEG structures are normally semicrystalline and their incorporation into cross-linked networks normally inhibits the crystallization. Among the starting materials, the ether based diallylic PEG **3P** was found to exhibit the highest degree of crystallinity with a crystallization enthalpy (ΔH_c) of 125 J g^{-1}. This is considerably high because pure PEG with $M_n = 1000$ g mol^{-1} has a ΔH_c of 165 J g^{-1} (34), which implies that the crystallization is not impaired to any larger extent by the allyl ether end-groups. Furthermore, the introduction of ester bonds decrease crystallization temperatures (T_c), crystallization enthalpies as well as the melting temperatures (T_m) and melting enthalpies (ΔH_m). In fact, in the case of ester based diallylic PEG **2P** crystallization does not occur during the cooling cycle; instead it shows a glass transition and crystallizes only during the heating cycle, indicating that the crystallization is severely hindered by the ester groups. When evaluating the DSC results from the cured films, it is evident that cross-linked networks hinder the PEG chains from crystallization. The only coating that displays a T_c and a T_m is coating **H8**, which contains **3P** with the highest crystallization enthalpy. Thermal analysis of the cured films shows that coating **H1** has a different structure than the other films as the T_g is significantly higher than in any of the other systems. For example, comparing **H1** ($T_g = -2.9$ °C) to its allyl ether

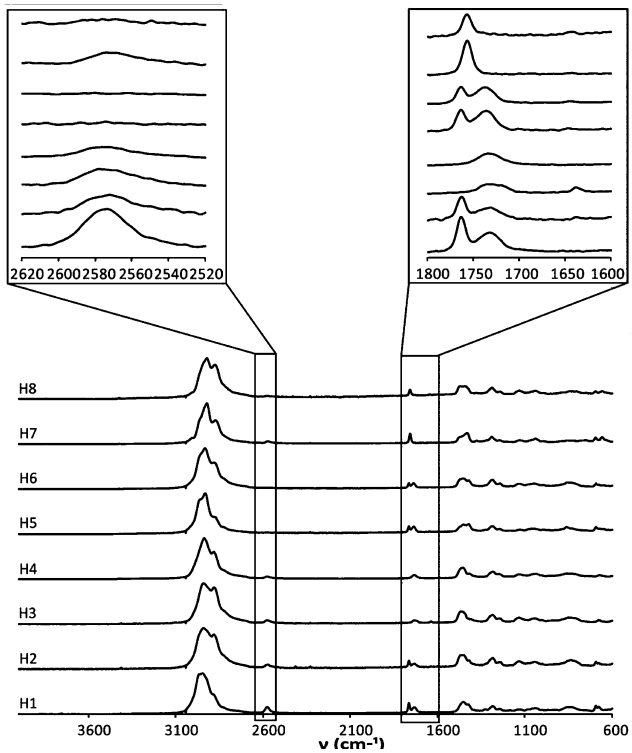

FIGURE 2. FT-Raman spectra of all hydrogel coatings H1−H8 with zoomed regions of interest displaying the absorption areas for thiols (2620−2520 cm^{-1}), triazine carbonyls (1775−1750 cm^{-1}), ester carbonyls (1750−1700 cm^{-1}), and allyls and methacrylates (1650−1600 cm^{-1}).

analogues **H5** ($T_g = -24$ °C) and **H7** ($T_g = -39$ °C), it is evident that there is a big difference in structure which can be explained by the presence of homopolymerization of the methacrylated groups. These results are in good accordance with the works of Cramer et al. and Lecamp et al. which have shown that the T_g of pure methacrylate systems are lowered by the addition of thiols. In fact, all of the thiol-methacrylate coatings formulated herein have a higher T_g than their allylic equivalents. This indicates there presence of homopolymerization in coatings **H1−H4** as indicated by the FT-Raman results.

Swelling and Degradation. The contact angles of the cured films, which were determined ahead of immersion (Table 1), reveal that a longer PEG chain decreases the contact angle in systems **H1** and **H2** as well as **H5** and **H6**. Comparing systems **H3** and **H4**, which also have the lowest contact angles, the result is the opposite. **H3** with a longer PEG chain than **H4** displays a higher contact angle that might be due to the fact that the **H3** coatings contain ca. 15% of unreacted hydrophobic methacrylic groups. Another reason for a higher contact angle is the observation of top curing, which gave coatings with rough surfaces. This phenomenon was also exhibited in systems **H7** and **H8** in which the surface roughness, and not the PEG length, significantly affect the contact angle results.

To evaluate the stability, all coatings were submerged into DIW as well as ASW and their swelling/degradation was followed by gravimetric analysis in combination with contact angle measurements. All systems expressing short PEG chains swelled to a lesser extent than systems based on the longer PEG chains. This is due to the more rigid network structure in the coatings with short PEG chains. System **H3**, which theoretically should have the greatest ability to swell because of the PEG spacers in the cross-linker **6**, swells to a lesser extent than **H2** and **H8** and reaches a plateau in 70% weight increase after 9 days in DIW, which is consistent throughout the whole test. This may be explained by the poor curing of **H3** where both some thiols and methacrylates remained unreacted after curing. In DIW (Figure 3), the systems based on short PEGs are more or less stable (less than 10% weight increase) throughout the whole test period. Only system **H1** swells to a greater extent than 10%, and a relatively large degree of swelling can be seen only between day 15 and the last point of measurement, day 28. In ASW (Figure 4), the situation is somewhat different; **H4** increases in weight throughout the test, in similarity to its analogue with long PEG chains, **H3**, ending up with a 100% weight increase after 28 days. **H1**, on the other hand, does not swell at all and the weight loss increases with time. Systems **H5** and **H7** seem, however, to behave in a similar fashion in both DIW and ASW. A clear trend that can be exemplified by the behavior of system **H6** in ASW is the initial swelling whereby some of the weak ester bonds from **AEOBA** are broken, leading to a looser network with a greater swelling ability. Further degradation, which occurs after 5 days, leads to material leakage, which results in a weight loss. Evidence of ester degradation can, in some cases, be seen in IR analysis by the presence of spectral bands corresponding to the O−H stretch of a carboxylic acid. However, this is often hard to detect, as degradation adducts also lead to external migration from the coating. As an illustrative example, FT-IR spectra of freshly prepared **H2** and **H2** submerged for 42 days in DIW and ASW are shown in Figure 5 (spectra of all compounds can be found in the Supporting Information). In DIW, the coating remains unaffected, whereas in ASW, the spectra have changed significantly, showing evidence of carboxyls present by the small shoulder at 3660 cm^{-1}. The coating release from the glass slides, which was observed in many of the more swollen systems, is most likely due to the hydrolysis breaking of sensitive silane primer (Si−O) bonds (35). This peeling process further complicates the evaluation of the degradation process in which the release due to degradation of the Si−O bond can occur simultaneously with other degradation processes, e.g., the case of **H8**, where the swelling/degradation studies had to be aborted after 9 days because of complete peeling. The peeled films, however, were uniform to a much greater extent than their methacrylate counterpart **H2**. This indicates that **H8** hydrogel is more stable and relatively less affected by degradation than **H2** which is in agreement with the findings of Rydholm et al. (27), who reported on the presence of labile esters increases the rate of degradation. Nonetheless, the introduction of silane primers through a precoating process had a large impact on the coating mechanism compared to an untreated glass surface. Coatings on untreated slides detached within a few minutes when submerged into DIW. The

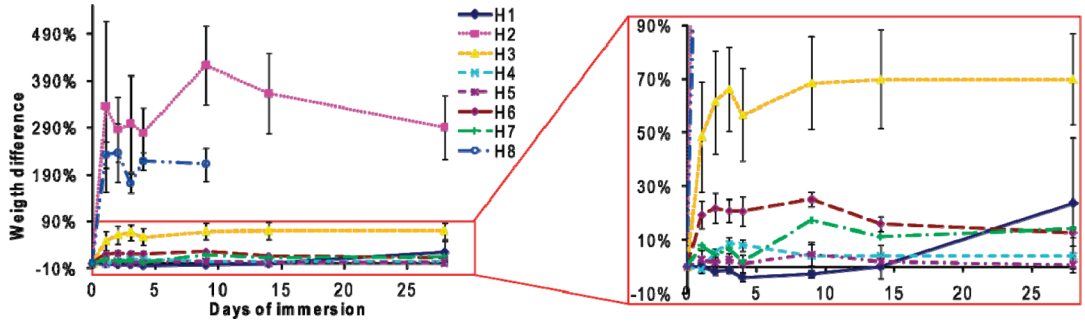

FIGURE 3. Results from the swelling experiments in DIW with an inset of the lower region of swelling.

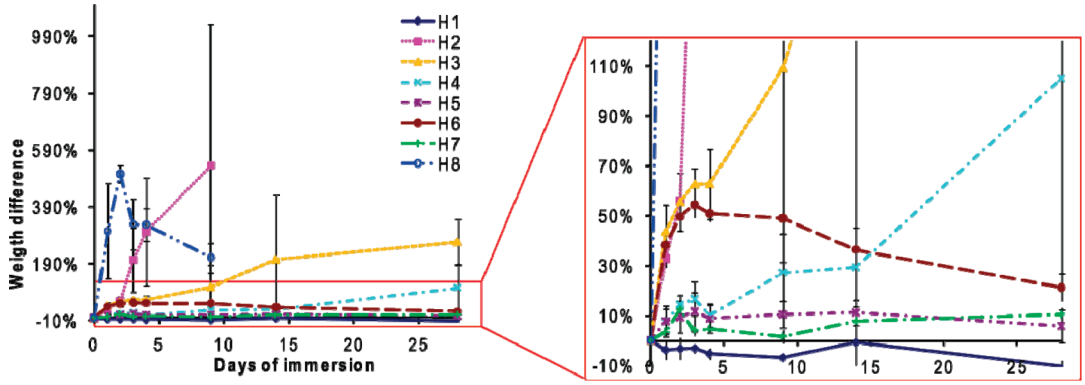

FIGURE 4. Results from the swelling experiments in ASW with an inset of the lower region of swelling.

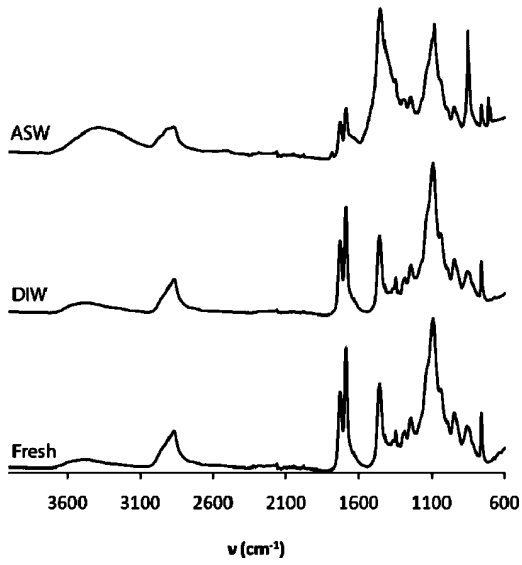

FIGURE 5. FT-IR of hydrogel coating H2, freshly prepared, after 42 days in DIW and 42 days in ASW.

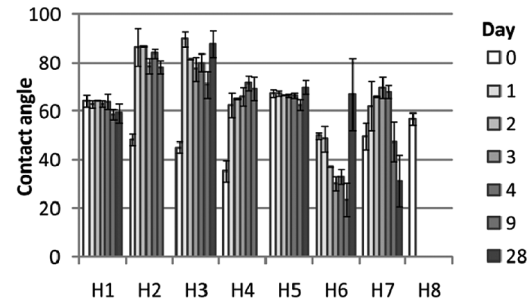

FIGURE 6. Contact angle measurements of coated slides for different periods of immersion in DIW.

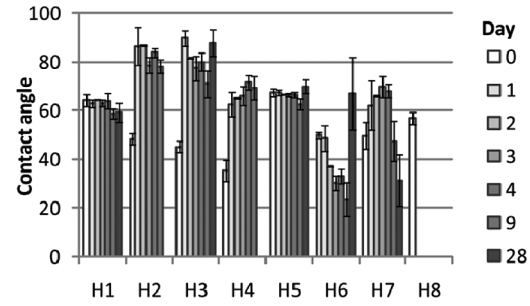

FIGURE 7. Contact angle measurements of coated slides for different periods of immersion in ASW.

swelling of the coatings with time and in DIW or ASW was also monitored by contact angle measurements (Figures 6 and 7). In DIW, all submerged hydrogels except **H1**, which does not change contact angle at all, showed an initial increase in contact angle followed by a plateau as seen in Figure 6. The increase in contact angle is most likely due to a change in surface morphology due to swelling, as the coatings that exhibit the highest swelling also display the highest increase in contact angle. In ASW, most coatings behave similarly to the coatings in DIW except for coatings **H6** and **H7**, which have an initial decrease in contact angle (Figure 7). Most coating systems have a lower contact angle after being submerged into ASW than into DIW, which can be explained as an effect of salt deposits on the coatings (12, 36).

Antifouling Properties. To evaluate the protein resistance, all swelled coatings **H1**−**H7** were initially incubated for 10 min with FITC-marked BSA in PBS and the total fluorescence was compared to nonincubated, swelled coatings. In addition to our coatings, polystyrene and acid-washed glass surfaces were used as references (Figure 8).

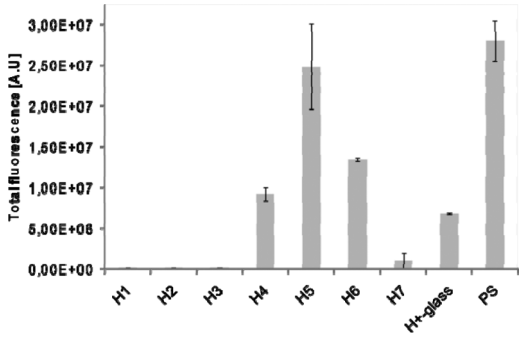

FIGURE 8. Results from the protein adsorption studies using FITC-labeled BSA in a PBS solution.

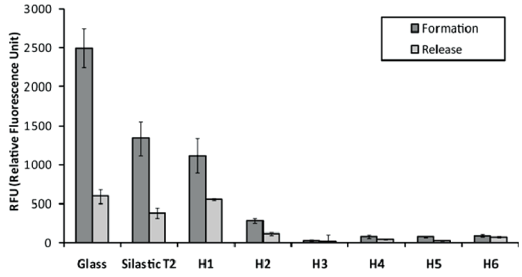

FIGURE 9. Results from the bioassay study with *Cobetia marina*.

Comparing the systems in pairs with respect to curing chemistry and cross-linker, the general conclusion is that systems with longer PEG chains render surfaces more resistant to protein adsorption. Moreover, the methacrylic systems **H1**, **H2**, **H3**, and the allylic ether-based system **H7** all display protein resistance while the allylic ester-based system **H5** and **H6** exhibit poor protein resistance. Systems **H5** and **H6**, exhibiting superior smoothness and optical transparency compared to the other hydrogel coatings, may influence the protein adsorption results. The surface morphology, being rough or smooth, plays a crucial role for the detection outcome through microscopy methods.

Furthermore, to evaluate the antifouling properties of our hydrogel systems as potential marine coatings, we used the marine bacteria *Cobetia marina* as a bioassay. In this case, acid-washed glass was used as hydrophilic reference and Silastic T2 as a hydrophobic reference (Figure 9). Fluorescence was measured before and after a dynamic phase in order to evaluate the fouling release properties in addition to the coating's direct antifouling properties. In this study, the coatings **H3** and **H4**, having the TMP-PEG based cross-linker **6**, performed best with respect to the inhibition of bacterial growth, closely followed by the ester-containing triazine-allyl ester systems **H5** and **H6**. The triazine-methacrylate coatings **H1** and **H2** do not perform as well as the other systems and **H1** is in fact the only coating that does not perform better than the references with respect to bacterial growth inhibition. When it comes to fouling release properties, the reference surfaces have the advantage and only **H5** has similar fouling release properties. Coatings **H1** and **H2** also present relatively good fouling release properties, whereas **H6** has the poorest fouling release properties. In general, it seems that a high fouling rate induces good fouling release properties.

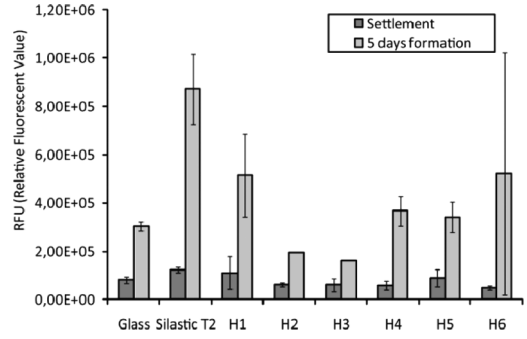

FIGURE 10. Results from the bioassay study with *Amphora coffeaeformis*.

Further bioassay testing was performed by studying the settlement and formation after five days of the diatom *Amphora coffeaeformis* (Figure 10). The tests show that the diatoms settle to a similar extent on all surfaces although some increased settlement can be seen on the hydrophobic reference Silastic T2. The systems with longer PEG chains (**H2**, **H3**, **H6**) and **H4** (PEG-based cross-linker) display a slightly lower settlement. Larger differences are seen after 5 days of formation, and the hydrophobic reference presents a significantly higher growth of the diatoms. Further study of Figure 10 reveals a clear trend in which the coatings with long PEG chains outperform the coatings with short PEG chains.

CONCLUSIONS

To investigate the antifouling potential of thiol-ene-based hydrogels, we efficiently constructed eight coating systems devided in four sets through thiol-ene coupling chemistry. By varying the length of the PEG chains, the nature of the vinylic end-groups, as well as the cross-linker, we accomplished a library of hydrogels with the presence or absence of hydrolytically degradable esters. Thiol-methacrylate coatings displayed evidence of homopolymerization during curing that displayed by the presence of unreacted thiols, whereas in the thiol-allyl ether coatings, the thiols were efficiently reacted according to Raman spectroscopy. Additionally, Higher T_g values were observed for the thiol-methacrylate coatings than the thiol-allyl coatings. Protein adsorption tests as well as the bioassay tests revealed improved antifouling performance with respect to longer PEG chains.

In summary, using thiol-ene chemistry, we have efficiently design an array of hydrogel coatings that comprised different structural building blocks. These coatings exhibited different hydrolytic stability with a variety of T_g values, which will allow further investigation of PEG-based coatings for antifouling applications.

Acknowledgment. The authors acknowledge the European Union's Sixth Framework Programme for financial support, Project COOP-CT-2006-032333. M.M. is grateful for the financial support from the Swedish Research Council (VR), Grant 2006-3617.

Supporting Information Available: FT-IR, FT-Raman spectra of the starting materials, and FT-IR of freshly cured

and degraded films (PDF). This material is available free of charge via the Internet at http://pubs.acs.org.

REFERENCES AND NOTES

(1) Yebra, D. M.; Kiil, S.; Dam-Johansen, K. *Prog. Org. Coat.* **2004**, *50*, 75–104.
(2) Almeida, E.; Diamantino, T. C.; de Sousa, O. *Prog. Org. Coat.* **2007**, *59*, 2–20.
(3) Hare, C. H. In *Protective Coatings—Fundamentals of Chemistry and Composition*; Hare, C. H. Ed.; Society for Protective Coatings: Pittsburgh, PA, 1998; pp 485—489.
(4) *Terms of Reference for a Corresponding Group on the Reduction of Harmful Effects of the Use of Antifouling Paints for Ships*; IMO-MEPC Paper MEPC 38/WP.6; U.S. Coast Guard: Washington, D.C., 1996.
(5) Hellio, C.; Yebra, D. In *Advances in Marine Antifouling Coatings and Technologies*; Hellio, C.; Yebra, D., Eds.; Woodhead Publishing Limited: Cambridge, U.K., 2009; pp 1—15.
(6) Wicks, Z. W.; Jones, F. N.; Pappas, S. P.; Wicks, D. A., In *Organic Coatings—Science and Technology*, 3rd ed.; Wicks, Z. W., Jones, F. N., Pappas, S. P., Wicks, D. A., Eds.; John Wiley & Sons: New York, 2007; pp 667—670.
(7) Cowling, M. J.; Hodgkiess, T.; Parr, A. C. S.; Smith, M. J.; Marrs, S. J. *Sci. Total Environ.* **2000**, *258*, 129–137.
(8) Cowie, P. R.; Smith, M. J.; Hannah, F.; Cowling, M. J.; Hodgkeiss, T. *Biofouling* **2006**, *22*, 173–185.
(9) Rasmussen, K.; Willemsen, P. R.; Ostgaard, K. *Biofouling* **2002**, *18*, 177–191.
(10) Rasmussen, K.; Ostgaard, K. *Water Res.* **2003**, *37*, 519–524.
(11) Gudipati, C. S.; Greenlief, C. M.; Johnson, J. A.; Prayongpan, P.; Wooley, K. L. *J. Polym. Sci., Part A: Polym. Chem.* **2004**, *42*, 6193–6208.
(12) Ekblad, T.; Bergstroem, G.; Ederth, T.; Conlan, S. L.; Mutton, R.; Clare, A. S.; Wang, S.; Liu, Y. L.; Zhao, Q.; D'Souza, F.; Donnelly, G. T.; Willemsen, P. R.; Pettitt, M. E.; Callow, M. E.; Callow, J. A.; Liedberg, B. *Biomacromolecules* **2008**, *9*, 2775–2783.
(13) Otsuka, H.; Nagasaki, Y.; Kataoka, K. *Adv. Drug Delivery Rev.* **2003**, *55*, 403–419.
(14) Andrade, J. D.; Hlady, V. *Adv. Polym. Sci.* **1986**, *79*, 1–63.
(15) Kingshott, P.; Griesser, H. J. *Curr. Opin. Solid State Mater. Sci.* **1999**, *4*, 403–412.
(16) Martens, P.; Anseth, K. S. *Polymer* **2000**, *41*, 7715–7722.
(17) Guo, K.; Chu, C. C. *J. Polym. Sci., Part A: Polym. Chem.* **2005**, *43*, 3932–3944.
(18) Lin-Gibson, S.; Jones, R. L.; Washburn, N. R.; Horkay, F. *Macromolecules* **2005**, *38*, 2897–2902.
(19) Malkoch, M.; Vestberg, R.; Gupta, N.; Mespouille, L.; Dubois, P.; Mason, A. F.; Hedrick, J. L.; Liao, Q.; Frank, C. W.; Kingsbury, K.; Hawker, C. J. *Chem. Commun.* **2006**, 2774–2776.
(20) Kolb, H. C.; Finn, M. G.; Sharpless, K. B. *Angew. Chem., Int. Ed.* **2001**, *40*, 2004–2021.
(21) Tornoe, C. W.; Christensen, C.; Meldal, M. *J. Org. Chem.* **2002**, *67*, 3057–3064.
(22) Rostovtsev, V. V.; Green, L. G.; Fokin, V. V.; Sharpless, K. B. *Angew. Chem., Int. Ed.* **2002**, *41*, 2596–2599.
(23) Hoyle, C. E.; Lee, T. Y.; Roper, T. *J. Polym. Sci., Part A: Polym. Chem.* **2004**, *42*, 5301–5338.
(24) Killops, K. L.; Campos, L. M.; Hawker, C. J. *J. Am. Chem. Soc.* **2008**, *130*, 5062–5064.
(25) Li, C. Y.; Birnkrant, M. J.; Natarajan, L. V.; Tondiglia, V. P.; Lloyd, P. F.; Sutherland, R. L.; Bunning, T. J. *Soft Matter* **2005**, *1*, 238–242.
(26) Reddy, S. K.; Anseth, K. S.; Bowman, C. N. *Polymer* **2005**, *46*, 4212–4222.
(27) Rydholm, A. E.; Reddy, S. K.; Anseth, K. S.; Bowman, C. N. *Polymer* **2007**, *48* (15), 4589–4600.
(28) Salinas, C. N.; Anseth, K. S. *Macromolecules* **2008**, *41*, 6019–6026.
(29) Aimetti, A. A.; Machen, A. J.; Anseth, K. S. *Biomaterials* **2009**, *30*, 6048–6054.
(30) Li, Q.; Zhou, H.; Hoyle, C. E. *Polymer* **2009**, *50*, 2237–2245.
(31) Moore, J. S.; Stupp, S. I. *Macromolecules* **1990**, *23*, 65–70.
(32) Cramer, N. B.; Bowman, C. N. *Polym. Prepr. (Am. Chem. Soc. Div. Polym. Chem.)* **2003**, *44*, 17.
(33) Lecamp, L.; Houllier, F.; Youssef, B.; Bunel, C. *Polymer* **2001**, *42*, 2727–2736.
(34) Pielichowski, K.; Flejtuch, K. *Polym. Adv. Technol.* **2002**, *13*, 690–696.
(35) Hong, H. G.; Jiang, M.; Sligar, S. G.; Bohn, P. W. *Langmuir* **1994**, *10*, 153–158.
(36) Chirila, T. V.; Gridneva, Z.; Morrison, D. A.; Barry, C. J.; Hicks, C. R.; Hill, D. J. T.; Whittaker, A. K.; Zainuddin, *J. Mater. Sci.* **2004**, *39*, 1861–1864.

AM900875G